

# Fabrication and characterization of methylammonium lead iodide-based perovskite solar cells under ambient conditions

Dwayne Jensen Reddy<sup>1</sup>, Ian Joseph Lazarus<sup>2</sup>

<sup>1</sup>Department of Electrical Power Engineering, Durban University of Technology, Durban, South Africa

<sup>2</sup>Department of Physics, Faculty of Applied Sciences, Durban University of Technology, Durban, South Africa

## Article Info

### Article history:

Received Feb 2, 2023

Revised Dec 11, 2023

Accepted Feb 16, 2024

### Keywords:

Bandgap

Electron transport layer

Methyl ammonium lead iodide

Perovskite solar cells

Titanium dioxide

## ABSTRACT

This study investigated the fabrication and characterization of  $\text{CH}_3\text{NH}_3\text{PbI}_3$  based perovskite solar cells (PSCs) using the one-step spin coating technique under ambient conditions, eliminating the need for expensive glovebox and thermal evaporation equipment. The perovskite layer was annealed at 65 °C for 30 seconds and 100 °C for 30 seconds, 1 and 2 minutes. The scanning electron microscope (SEM) images show a smooth and uniform surface coverage for the ETL and  $\text{CH}_3\text{NH}_3\text{PbI}_3$  layers. SEM results also show an average grain size of 397 nm for  $\text{CH}_3\text{NH}_3\text{PbI}_3$  and an average particle size of ~17 nm for  $\text{TiO}_2$  was confirmed by transmission electron microscopy (TEM). X-ray diffraction (XRD) results confirmed the formation of tetragonal perovskite ( $\text{CH}_3\text{NH}_3\text{PbI}_3$ ) phase with high crystallinity with a crystallite size of 19.99 nm for the samples annealed for 30 seconds at 65 °C and 1 min at 100 °C. FTIR results also confirmed the presence of anatase  $\text{TiO}_2$  at wavenumber 438  $\text{cm}^{-1}$  and the formation of the adduct of  $\text{Pb}_2$  with dimethyl sulfoxide (DMSO) and MAI is confirmed at 1,015  $\text{cm}^{-1}$ . From the Tauc plot the bandgap energy of  $\text{TiO}_2$  and Perovskite layers was determined to be 3.52 eV and 2.06 eV respectively. An open-circuit voltage was 0.9057 V and short circuit current density was 12.2185  $\text{mA}/\text{cm}^2$  with a fill factor of 48.05 and power conversion efficiency (PCE) of 5.199%.

This is an open access article under the [CC BY-SA](https://creativecommons.org/licenses/by-sa/4.0/) license.



## Corresponding Author:

Ian Joseph Lazarus

Department of Physics, Faculty of Applied Sciences, Durban University of Technology

Durban, South Africa

Email: lazarusi@dut.ac.za

## 1. INTRODUCTION

Perovskite solar cells (PSC) has attracted much interest in recent years from researchers due to its potential as a next generation thin film solar technology. The attract features of PSC include high efficiency, low manufacturing costs, versatility and flexibility. This opens up the possibilities of applications in building integrated photovoltaics (BIPV), wearable electronics and integration into curved or irregular shaped structures.

The absorbing material of PSC devices with the generic crystal structure  $\text{ABX}_3$  is referred to as perovskite [1]. So far, the most efficient PSC devices have been created using the following materials in the perovskite form of  $\text{ABX}_3$  with methyl ammonium ( $\text{CH}_3\text{NH}_3$ ) as (A), metal like lead (Pb) or tin (Sn) as (B), and a halide bromide ( $\text{Br}_3$ ), iodide ( $\text{I}_3$ ), or chloride ( $\text{Cl}_3$ ) as  $\text{X}_3$  [2]. This perovskite material has the following attractive features: a low bandgap that allows lighter to be absorbed, a high carrier charge mobility that allows the created electron and hole to move through the material without much resistance, and a high diffusion length that prevents electron-hole pair recombination [3].

As depicted in Figure 1, light is transmitted through the fluorine doped tin-oxide (FTO) and electron transport layer ( $\text{TiO}_2$ ) and absorbed by the perovskite layer to cause charge separation. This process excites an electron into the conduction band and creates a hole (positive charge) in the valence band. While the electrons are injected into the electron-transport layer and the holes into the hole-transport layer (Spiro-OMeTad), the positive holes in the cathode layer are filled by the electrons after they have passed via an external circuit. As shown in Figure 1, a closed-circuit cell is created by connecting the transparent FTO electrode and the rear contact metal electrode [4], [5].

With a record PCE of 22.1%, metal halide perovskite (MHP) solar cells have shown the fastest rate of improvement in power conversion efficiency (PCE) among all photovoltaic technologies to date. MHP solar cells are now as efficient as silicon solar cells [6]. Additionally, earth-abundant compositions and inexpensive solution processing techniques can be used to create MHP solar cells. As a result, they have a stronger chance of realizing more competitive solar cell power technology from an economic perspective [7].

Much of the improvements to the performance of perovskite can be attributed to the refinement of the perovskite layer fabrications protocols. There have been several techniques developed such as the one-step, two-step spin coating solution method, solvent engineering method, anti-solvent engineering method as well as vacuum and vapor-assisted methods. The spin coating solution method is considered the most affordable deposition technique for research purposes which allows for fairly uniform surface coverage. Both the one and two-step deposition techniques for  $\text{CH}_3\text{NH}_3\text{PbI}_3$  were investigated by Ahn *et al.* [8] and Im *et al.* [9]. Ahn *et al.* [8] showed that for the one-step method, the  $\text{CH}_3\text{NH}_3\text{PbI}_3$  perovskite precursor solution was annealed at  $40^\circ\text{C}$  for 3 min and  $100^\circ\text{C}$  for 5 min to obtain a PCE of 7.5%. For the two-step method under the same annealing setting Im *et al.* [9] achieved a PCE of 13.9%. For a similar  $\text{CH}_3\text{NH}_3\text{PbI}_3$  perovskite precursor composition, Ozaki *et al.* [10] achieved a PCE of 20.3% using the one-step method with an annealing setting of  $40^\circ\text{C}$  for 5 min,  $55^\circ\text{C}$  for 5 min, and  $75^\circ\text{C}$  for 5 min and  $100^\circ\text{C}$  for 30 minutes. By applying an anti-solvent during the last 2 seconds of the perovskite spin coating stage the desired high crystalline formation of tetragonal crystal structure perovskite was formed. Regardless of the method, a high degree of crystallinity, flat and dense perovskite layers are critical for low surface defects, energy losses, and high-power conversion efficiency. These characteristics play a vital role in minimizing the formation of pinholes and short-circuiting of the PSC device. However high efficiency and reproducible PSCs are fabricated using expensive deposition equipment, a clean room, glovebox, and thermal evaporation equipment which can limit research in the development of PSCs.

It is within this context of varying reports of annealing time at  $100^\circ\text{C}$  that we focused on the widely used  $\text{CH}_3\text{NH}_3\text{PbI}_3$  as the perovskite material developed with the one-step spin coating method and anti-solvent technique for an investigation into the crystal structure and performance under different annealing settings. The perovskite layer was annealed under three different settings of  $65^\circ\text{C}$  for 30 s and  $100^\circ\text{C}$  for 30 s,  $65^\circ\text{C}$  for 30 s and  $100^\circ\text{C}$  for 1 minute and  $65^\circ\text{C}$  for 30 s and  $100^\circ\text{C}$  for 2 minutes under ambient conditions. Modified spin coating parameter setting, perovskite annealing setting, and vacuum storage are provided to reliably fabricate and reproduce PSCs. After applying these methods a maximum PCE of 5.199% was achieved with reliability and reproducibility. The paper structure is as follows; in section 2 the fabrication method is presented. In section 3 we present the performance results and discussion of the characterization techniques used to determine the structural, morphological and optical properties. Our observations and recommendations are concluded in section 4.

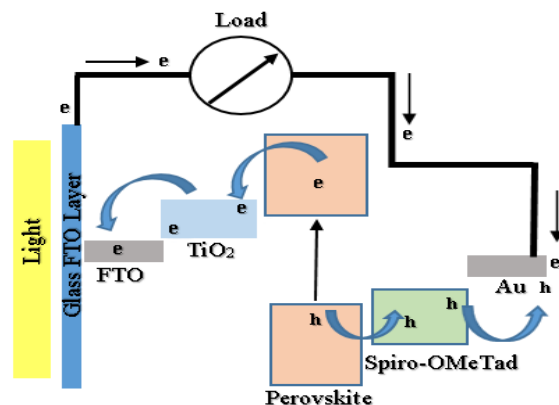


Figure 1. Typical PSC planar architecture and operation

## 2. CHEMICALS AND FABRICATION METHOD

### 2.1. Chemicals

The electron transport layer consisted of Titanium isopropoxide (TTIP), ethanol (EtOH, super dehydrated,) and hydrochloric acid (HCL). The perovskite absorber layer consisted of Methyl ammonium iodide (MAI, 99%), Lead (II) Iodide (PbI<sub>2</sub>, 99.9%), dimethylformamide (DMF, super hydrated), dimethylsulfoxide (DMSO, super hydrated), di-ethyl ether. The hole transport layer consisted of 2, 2', 7, 7'-Tetrakis (N, N-di-p-methoxyphenylamino)-9, 9'- Spirobifluorene (Spiro- OMeTAD powder), 4- Tert – Butylpyridine (TBP, 96%), Bis (trifluoromethane sulfonimide lithium salt (LiTFSI), chlorobenzene. All chemicals were purchased from Sigma- Aldrich Co.

### 2.2. Device fabrication

All layers of the PSC shown in Figure 2 were fabricated under ambient conditions, relative humidity was maintained at < 65% at a controlled room temperature of (~20°C) and was adapted and modified from [8]–[10]. Step 1: Fluorine-doped tin oxide glass substrates (25 mm x 25 mm) were cleaned in beakers containing detergent and deionized water, and ultrasonically cleaned in ethanol for 20 minutes at 80 °C. Substrates were carefully removed and rinsed in deionized water, dried on a hotplate and then placed in a UVO cleaner for 15 minutes for further cleaning before depositing the TiO<sub>2</sub> layer. A piece of tape was placed 5 mm from the top edge, leaving the front FTO anode contact exposed and leaving 20 mm x 20 mm space available for the depositing of the precursor solutions.

Step 2: the 0.22M, TiO<sub>2</sub> electron transport layer precursor solution was prepared by vigorously stirring 14.29 ml of ethanol and 0.28 ml of 2M HCL on a magnetic stirrer for 30 minutes, 1 ml of TTIP was added dropwise to this solution and was allowed to stir vigorously for 2 hours at room temperature. The TiO<sub>2</sub> precursor solution was then filtered using a 0.45 µm Teflon filter before spin coating to ensure the solution was free of any undissolved particles thus ensuring a smooth and uniform surface coverage was obtained. The 300 µl TiO<sub>2</sub> solution was dynamically spin-coated on the UVO-treated FTO at 1000 rpm for 15 seconds and annealed to 550 °C for 30 minutes to form a transparent, smooth, and homogeneous electron transport thin film layer as shown in Figure 2(a).

For the synthesis of the TiO<sub>2</sub> nanoparticles, the remaining 0.22 M solution was then left to age for ~72 days until a clear and transparent gel is formed. The gel was placed in a hot air dryer for 12 hours at a temperature of 80 °C to form a dry TiO<sub>2</sub> powder. The dried TiO<sub>2</sub> powder is then placed in a furnace and heated to 550 °C for 30 minutes to form anatase TiO<sub>2</sub> nanoparticles for Fourier transform infrared spectroscopy (FTIR), X-ray diffraction (XRD), and transmission electron microscopy (TEM) characterization.

Step 3: the perovskite absorber layer was prepared by dissolving 0.16 g methyl ammonium iodide and 0.46 g lead iodide into 0.08 ml dimethyl sulfoxide (DMSO) and 0.6 ml DMF. This was stirred for ~24 hours to ensure a homogenous solution before deposition onto the TiO<sub>2</sub> layer. The TiO<sub>2</sub> layer was UVO treated again for 15 minutes before spin-coating 250 µl of the perovskite solution at 5000 rpm for 15 seconds with 350 µl of di-ethyl ether slowly dripped from approximately 2cm away from the rotating substrate during the last 5 seconds. The coated surface was placed on a digital hotplate at 65 °C for 30 seconds then slowly ramped up to 100 °C and annealed for 1 minute to form the dark brown and transparent perovskite layer shown in Figure 2(b). This was then transferred immediately into a vacuum desiccator before deposition of the hole transport layer (HTL) to minimize the effects of degradation of the perovskite layer due to humidity.

Step 4: the HTL was prepared by dissolving 0.52 g of LiTFSI in 1 ml acetonitrile and stirred vigorously for 10 minutes to form the LiTFSI stock solution. Then 0.07g of Spiro-OMeTAD powder was added to 1 ml chlorobenzene and stirred vigorously for 10 minutes to form the Spiro-OMeTAD solution. Thereafter 0.03 ml of tBP and 0.02 ml of the LiTFSI solution was added to the Spiro-OMeTAD solution and stirred for 30 minutes to form the HTL precursor solution. Lastly, 200 µl of the HTL solution was dynamically spin-coated on top of the perovskite layer at 1000 rpm for 15 seconds and placed in a vacuum desiccator to oxidize overnight, before the immediate application of 8 mg activated carbon powder and FTO as the back conductive cathode contact (steps 5 & 6) with binder clips to hold the PSC together shown in Figure 2(c). This allowed minimum exposure of our cells to environmental conditions and performance reduction. The complete step-by-step fabrication is shown in Figure 2(d).

### 2.3. Characterization equipment

The identification of the functional groups was acquired by Agilent Cary 630 attenuated total reflectance-Fourier transform infrared (ATR-FTIR) using a diamond crystal operating between 400-4000 cm<sup>-1</sup>. The X-Ray Diffractometer, model: D8 Advanc, make: M/s Bruker AXS, Germany was used to determine the perovskite structure. The surface morphology properties and elemental percentage concentration was

characterized by the Zeiss scanning electron microscope (SEM) operating at 40 kV and 40 mA and energy dispersive X-Ray (EDX). Particle size was determined by TEM using Image J software. The optical properties were obtained by the agilent Cary 60 UV-Vis-NIR spectrometer. Bandgaps were calculated using the Tauc plot with a direct bandgap power factor. The photovoltaic properties were measured with a Keithley 2460 source measuring unit and an illumination light source of AM 1.5 (100 mW/cm<sup>2</sup>).

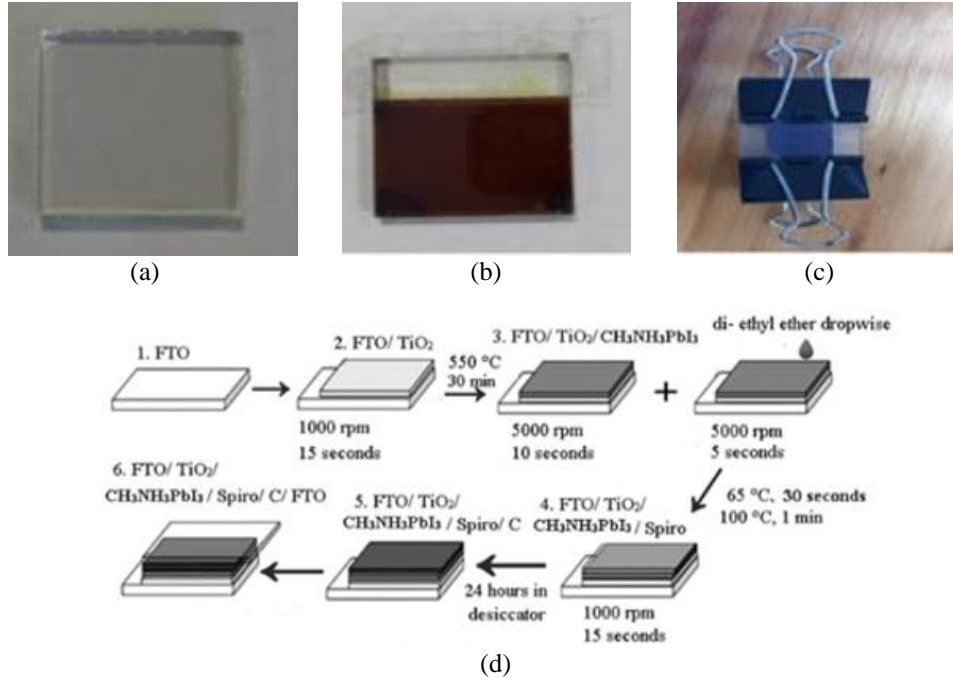


Figure 2. Perovskite solar cell fabrication; (a) TiO<sub>2</sub> spin coated on FTO glass substrate, (b) methyl ammonium lead iodide spin-coated and annealed on TiO<sub>2</sub> layer, (c) completed PSC, and (d) fabrication steps of PSC

### 3. RESULTS AND DISCUSSION

#### 3.1. X- Ray diffraction: structural properties of CH<sub>3</sub>NH<sub>3</sub>PbI<sub>3</sub>

The XRD results of perovskite films annealed at 65 °C for 30 seconds and then annealed at 100 °C for 30 s, 1min, and 2 minutes are presented in Figure 3. Strong peaks at 14.06° (110), 28.15° (220) and 31.68° (312) indicate the formation of tetragonal perovskite (CH<sub>3</sub>NH<sub>3</sub>PbI<sub>3</sub>) phase [11] with high crystallinity for the samples annealed for 30 sec and 1 min. This verified the annealing settings of the work done by Ahn *et al.* [8] and was used for further characterization of the material’s properties. According to Figure 3 the lead iodide phase in the XRD pattern of the sample annealed for 30 sec may be due to the residual phase from preparation which remains within the bulk of the material. In other words, the annealing time was not sufficient to completely convert the precursors to the perovskite phase. For the sample annealed for 2 min, the peaks at 13.59° (001), 27.58° (101), 30.49° (102), 43.52° (111), 50.17° (201), and 73.57° (105) correspond to hexagonal lead iodide phase (JCPDS No. 07-0235) [12]. The PbI<sub>2</sub> phase is formed due to the decomposition of the perovskite phase upon annealing at 100 °C, where methyl ammonium iodide (CH<sub>3</sub>NH<sub>3</sub>I) escaped from the Perovskite film to form lead iodide by heating for a longer time (2 min). It was found previously that during the annealing process, CH<sub>3</sub>NH<sub>3</sub>I can escape if annealed too long ,especially for some loosely bonded Perovskite phases [13], [14].

The average crystallite size of the under-studied samples was calculated by resolving the characteristic peaks using Debye-Scherer’s formula [15]:

$$D = K\lambda / \beta \cos(\theta) \tag{1}$$

where K is the shape factor (0.9), D is the average crystallite size, β is the half-width of the measured diffraction peak, θ is the diffraction angle, and λ is the X-ray wavelength (0.154 nm). The crystallite size for the perovskite phase was equal to 14.32 nm and 19.99 nm for the samples annealed at 65 °C for 30 s and 100 °C for 30 s and 65 °C for 30 s and 100 °C for 1 min, respectively. In addition, the crystallite size of the PbI<sub>2</sub> phase in the sample annealed at 65 °C for 30 s and 100 °C for 2 min was 12.21 nm. The more intense

characteristic peaks and larger average crystal size after 65 °C for 30 s and 100 °C for 1 min annealing time attributed to the improved crystallinity or composition homogeneity with fewer low-dimensional defects and less scattering between grain boundaries in the solvent-annealed perovskite film.

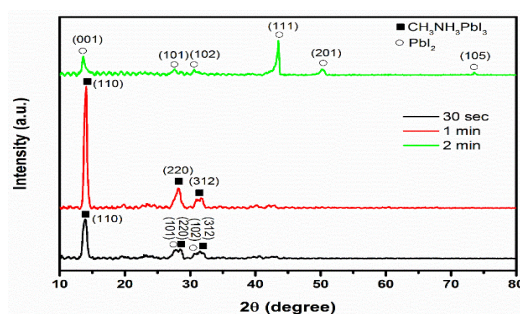


Figure 3. XRD patterns of Perovskite films annealed at 65 °C for 30 s and 100 °C for 30 sec, 65 °C for 30 s and 100 °C for 1 min, 65 °C for 30 s and 100 °C for 2 min

### 3.2. Fourier transform infrared spectroscopy: identification of functional groups

In the FTIR spectrums shown in Figure 4, it can be seen from Figure 4(a) that there is no presence of O-H hydroxyl groups, in the range of wavenumber 3100-3600  $\text{cm}^{-1}$  which can be attributed to the high calcination temperature of 550 °C. The hydroxyl groups could interact with the  $\text{NH}_4$  and  $\text{CH}_3$  in the perovskite causing the decomposition of  $\text{CH}_3\text{NH}_3\text{PbI}_3$  into  $\text{PbI}_2$  and  $\text{CH}_3\text{NH}_3\text{I}$  which will lead to reduced performance of the PSC. The sharp peaks between 528-408  $\text{cm}^{-1}$  indicate that the thin film is well crystallized and is assigned to O-Ti-O bonding. The sharp peak at 438  $\text{cm}^{-1}$  is characteristic of  $\text{TiO}_2$  anatase [16]–[19].

FTIR spectroscopy was conducted to identify  $\text{CH}_3\text{NH}_3\text{PbI}_3$  formation. The FTIR spectra in Figure 4(b) feature vibrational modes at 3116  $\text{cm}^{-1}$  (N-H stretch), 3116-1569  $\text{cm}^{-1}$  (C-H stretch), 1569  $\text{cm}^{-1}$  (antisymmetric  $\text{NH}_3^+$ ), 1458  $\text{cm}^{-1}$  (symmetric  $\text{NH}_3^+$  bend), 1015  $\text{cm}^{-1}$  (MAI· $\text{PbI}_2$ ·DMSO), 950  $\text{cm}^{-1}$  (C-N stretch) and 907  $\text{cm}^{-1}$  ( $\text{NH}_3^+$ / $\text{CH}_3$  rock) which is similar to related literature [19]–[23]. The adduct of  $\text{Pb}_2$  with DMSO and MAI is confirmed by FTIR spectroscopy at 1015  $\text{cm}^{-1}$ .

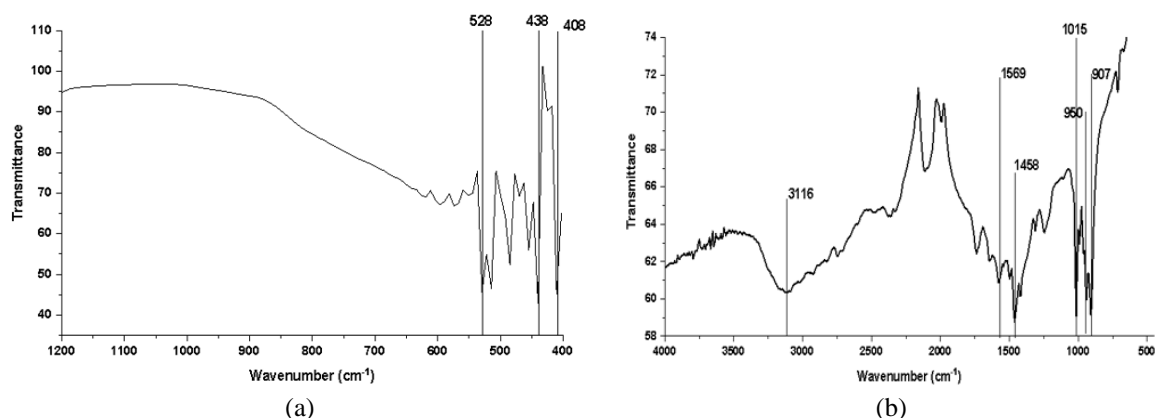


Figure 4. FTIR spectra (a) FTIR spectra of planar  $\text{TiO}_2$  thin film annealed at 550 °C and (b) FTIR spectra of perovskite thin film

### 3.3. SEM, TEM and EDX: morphological properties and elemental weight percentage compositions

The surface morphology and particle size of the  $\text{TiO}_2$  layer shown in Figure 5. Figure 5(a) was observed by scanning electron microscope. The surface morphology of the thin films annealed at 550 °C under ambient conditions showed a relatively uniform surface coverage with densely packed  $\text{TiO}_2$  nanoparticles confirmed by the TEM results shown in Figure 5(b). Figure 5(c) shows the morphology and size distribution of the  $\text{TiO}_2$  nanoparticles ranging from 5 to 30 nm. To characterize the surface roughness of the  $\text{TiO}_2$  and Perovskite layers, the image J software tool was utilized on the SEM images. The estimated root

mean square (RMS) roughness of 21.9 nm was obtained for the TiO<sub>2</sub> layer indicating a fairly smooth layer coverage; however, an ultra-smooth surface is imperative to achieve better performance as reported by [24], [25]. This allows for a smoother surface for the deposition of the perovskite layer and minimizes the formation of defects. The histogram in Figure 5(d) shows that the average particle size of TiO<sub>2</sub> nanoparticles synthesized was ~ 17 nm.

The SEM images of the CH<sub>3</sub>NH<sub>3</sub>PbI<sub>3</sub> thin film and elemental composition is presented in Figure 6. Figure 6(a) shows a dense and well-interconnected layer with particle sizes ranging from 50 nm to 800 nm with an average particle size of 397 nm shown in Figure 6(b). The estimated root mean square (RMS) roughness of 31.75 nm shown in Figure 6(c) was obtained for the Perovskite layer. Highly dense CH<sub>3</sub>NH<sub>3</sub>PbI<sub>3</sub> films were formed by the rapid evaporation of DMF with diethyl ether while spinning for the last 5 seconds [10]. Energy dispersive X-ray spectrometry analysis of FTO/TiO<sub>2</sub>/CH<sub>3</sub>NH<sub>3</sub>PbI<sub>3</sub> thin films was performed to determine and identify the elemental composition and weight percentage (wt %) concentrations. Figure 6(d) shows peaks for Ti, O, Sn, I, Pb. The presence of Si is due to the FTO-coated quartz substrate used; no other impurities are seen.

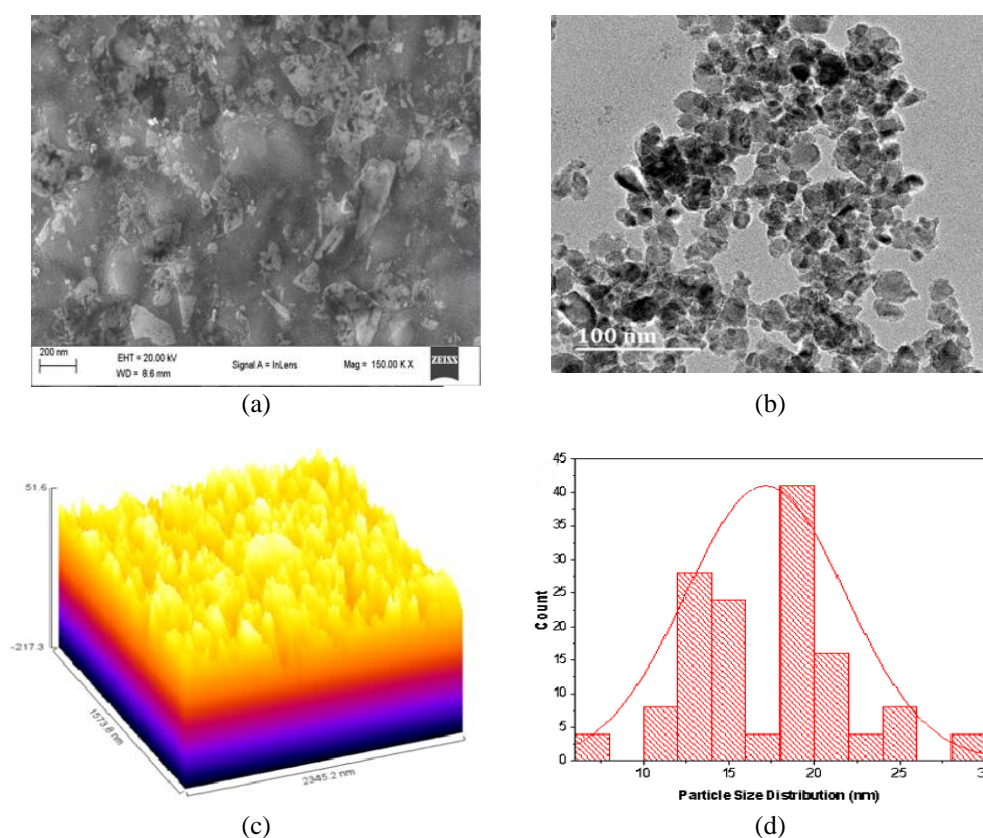


Figure 5. Surface and particle imaging of TiO<sub>2</sub>; (a) SEM image of TiO<sub>2</sub> surface layer, (b) TEM image of TiO<sub>2</sub> nanoparticles, (c) surface roughness of TiO<sub>2</sub> layer, and (d) TiO<sub>2</sub> nanoparticle size distribution

### 3.4. UV-Vis spectroscopy: optical properties

The UV-Vis transmission and absorption spectra shown in Figure 7 were obtained using a Cary 60 UV-Vis. Figure 7(a) shows the UV-VIS transmission spectra of the FTO and TiO<sub>2</sub> thin films. The UV-Vis transmission spectra for the TiO<sub>2</sub> thin film indicate a ~10% drop in transmission from ~80% for FTO to ~70% from the visible light to near-infrared regions. The TiO<sub>2</sub> layer has a significantly lower absorbance in the 300 nm to 800 nm wavelength range as expected when compared to the perovskite layer. The UV-Vis absorption spectra in Figure 7(b) shows a redshift to near infrared in the absorption range with the introduction of the perovskite layer. The CH<sub>3</sub>NH<sub>3</sub>PbI<sub>3</sub> shows good light absorption with a bandgap of ~2.06 eV from the visible light to near-infrared regions. The decrease in bandgap and increase in fermi energy allows electrons to move more freely from the valence to the conduction band. The bandgap ( $E_g$ ) of the thin film samples was calculated using the Tauc plot method. The bandgap energy of 3.52 eV for TiO<sub>2</sub> and 2.06 eV for perovskite was measured by plotting  $(\alpha/h\nu)^2$  as a function of photon energy, and extrapolating the linear region of the absorption curve as shown in Figure 7(c).

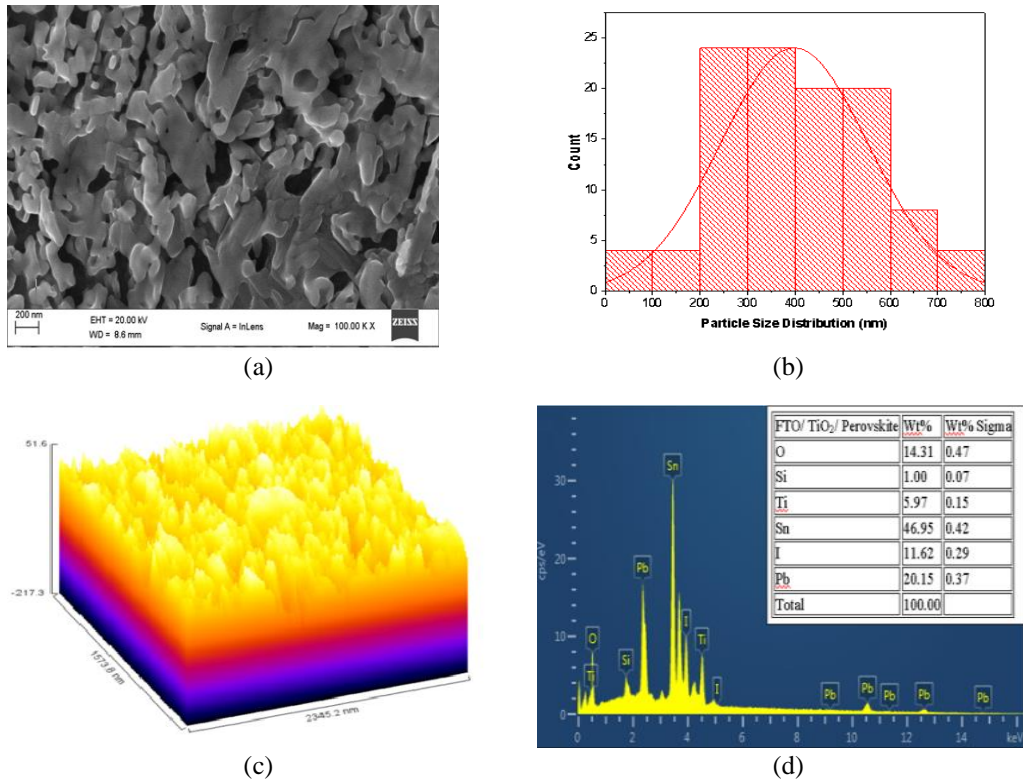


Figure 6. Perovskite surface and elemental composition; (a) SEM image of the Perovskite surface layer, (b) perovskite particle size distribution, (c) surface plot of Perovskite layer, and (d) elemental composition of the FTO/TiO<sub>2</sub>/Perovskite layers

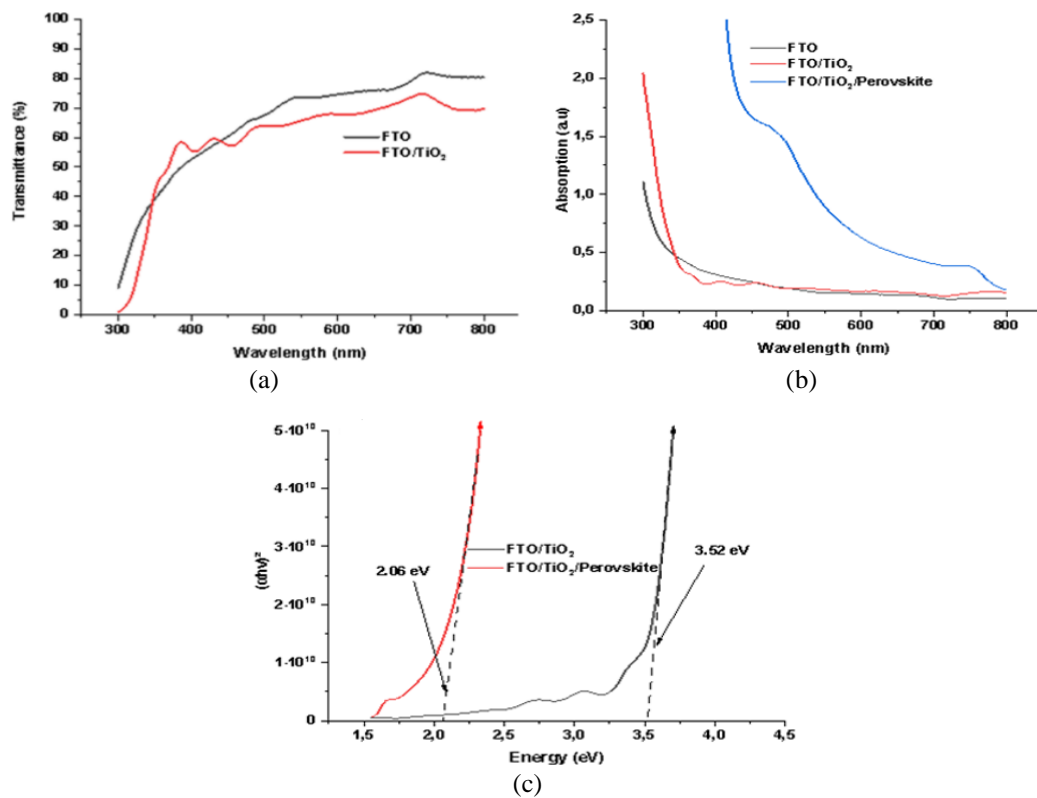


Figure 7. UV-Vis spectra; (a) transmission spectra FTO and FTO/ TiO<sub>2</sub> layer, (b) absorption spectra of FTO, FTO/TiO<sub>2</sub> and FTO/TiO<sub>2</sub>/Perovskite, and (c) band gap energy of TiO<sub>2</sub> and Perovskite material

### 3.5. PSC performance

The open-circuit voltage (when current is zero), short-circuit current density (when voltage is zero), the voltage at maximum power point ( $V_{mpp}$ ), and current density at maximum power point ( $J_{mpp}$ ) values serve as important electrical parameters in determining the efficiency of converting sunlight to electricity in a solar cell. The performance measurements shown in Figure 8 were taken using a Kiethley 2460 source measuring unit at one sun ( $100 \text{ mW/cm}^2$ ). The solar cell device described was tested on an active area  $0.1 \text{ cm}^2$  and gave an open-circuit voltage ( $V_{oc}$ ) of  $0.9057 \text{ V}$ , short circuit current density up to  $12.2185 \text{ mA/cm}^2$ , PCE of  $5.199\%$  and fill factor of  $48.05$  was achieved in our device, compared to the fabrication of a vapour-assisted PSC solar cell under similar conditions of  $0.972 \text{ V}$ ,  $17.5 \text{ mA/cm}^2$ , PCE of  $11\%$ , and fill factor of  $65.2$  [26]. The voltage and current density at the maximum power point were  $0.5763 \text{ V}$  and  $9.8213 \text{ mA/cm}^2$  respectively, resulting in a maximum power output of  $5.2 \text{ mW}$ . Energy losses in voltage and current occur due to the method of deposition, surface defects, increasing internal recombination of charge carriers, and bandgap misalignment between the ETL- Perovskite-HTL interfaces limiting charge transport,  $V_{oc}$  and PCE [27].

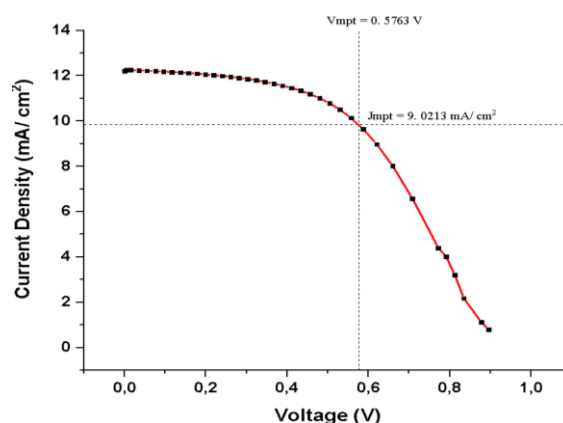


Figure 8. J-V curve for PSC

## 4. CONCLUSION

It has been shown that PSCs can be fabricated without expensive equipment under ambient conditions by carefully considering ambient and process parameters. In order to ensure the reliability and validity of our experimental setup, we replicated the results of our experiments to investigate how each PSC layer could be modified to address the problems identified. During spin coating, it is noted that tape protection of the FTO anode contact has limitations, including incomplete surface coverage, uneven surface coating, reduced active area, and edge effects, resulting in lower PCE and performance. For large cells and commercial viability, this leads to scalability issues. Optimization of the spin coating parameters (spin speed, duration, solution concentration), and etching off a small area of FTO, will decrease the active area and allow an exposed area for a back contact. This can reduce the effects mentioned and achieve a more even surface thickness and uniform coverage. Titanium dioxide annealed at a high temperature of  $\sim 550 \text{ }^\circ\text{C}$  consumes high amounts of electrical energy during annealing. Consequently, device fabrication is limited to solid substrates with good thermal properties. By investigating and optimizing low-temperature annealing materials for ETL layers, such as  $\text{SnO}_2$ , we will be able to anneal onto flexible substrates like polyester (PET) and develop flexible PSCs allowing for a wide variety of applications.

The optimum annealing temperature time of the perovskite layer at  $100 \text{ }^\circ\text{C}$  using the anti-solvent method was verified and the corresponding material properties were presented and discussed. The structural, morphological, optical, and performance properties of the Perovskite absorber and  $\text{TiO}_2$  electron transport layers were systematically studied and presented.

The results show the formation of a highly crystalline tetrahedral structure for  $\text{CH}_3\text{NH}_3\text{PbI}_3$  via a one-step method, a well-interconnected surface layer, significant light absorption and a bandgap of  $2.06 \text{ eV}$ . The anatase phase of  $\text{TiO}_2$  was confirmed via FTIR at wavenumber  $438 \text{ cm}^{-1}$ . It had an average particle size of  $\sim 20 \text{ nm}$ , uniform thin film coverage, optical transmission of  $\sim 70\%$  and a bandgap of  $3.52 \text{ eV}$ . The PSC developed under the mentioned conditions achieved an open circuit voltage of  $0.9057 \text{ V}$ , short circuit current density of  $12.2185 \text{ mA/cm}^2$ , and PCE of  $5.199\%$ .

Perovskites are fabricated using toxic DMF solvents. Investigations into less toxic substitutes including N-methyl-2-pyrrolidone (NMP), ethyl acetate (EA) and DMSO, dimethyl propylene urea (DMPU) and 2-methyl tetrahydrofuran achieved promising results, although the drop in PCE indicates that solvent

engineering research is needed further. By looking at the effects of elemental doping on the ETL, absorber layer and HTL, fundamental properties of the ETL, absorber, and HTL layers can be improved. Through numerical analysis of SCAPS 1D improving fundamental PV properties can be achieved by including and optimizing the buffer layer between the ETL/Perovskite interface and the Perovskite/HTL interface.

Additionally incorporating a surfactant such as Triton X-100 into the ETL, absorber and HTL, can improve film quality, homogeneity, material properties and device performance. Adding small amounts of Triton X-100 surfactant to a triple cation mixed halide precursor solution improves film quality, surface coverage, wettability, crystallinity, and stability. The HTL precursor solution containing polyaniline poly(styrenesulfonate) can also be improved by adding Triton X-100, which results in an alternative, less costly, and low-temperature HTL option that improves hole extraction, film quality, and PCE.

As a result of their cost-effective processability and stability in large production processes, carbon-based electrodes are attractive alternatives to thermal evaporation of back metal contacts at high temperatures. There are, however, issues related to poor interface contact and inferior performance between perovskite and carbon electrodes that need to be explored in greater detail. As flexible carbon electrodes, graphene, carbon nanotubes, and carbon black have shown excellent resistance to mechanical deformation. Carbon-based electrodes for PSCs continue to face the challenge of interface contact. The recommendations and results indicate that further research into material combination optimization, surfactant engineering, elemental doping, and process optimization is required to further improve the fundamental properties of each layer of the PSC and its overall performance and stability for commercialization.

## ACKNOWLEDGEMENTS

The authors gratefully acknowledge the financial support from the South African National Research Foundation grant reference TTK200309508592.

## REFERENCES

- [1] R. L. Z. Hoyer *et al.*, "Perovskite-inspired photovoltaic materials: toward best practices in materials characterization and calculations," *Chemistry of Materials*, vol. 29, no. 5, pp. 1964–1988, Mar. 2017, doi: 10.1021/acs.chemmater.6b03852.
- [2] A. Farawar, "Perovskite solar cells: stability, design architecture, photophysical properties, and morphology of the film in organometal halide perovskite-based photovoltaics," no. November, p. 54, 2015, doi: 10.13140/RG.2.1.1406.8242.
- [3] N.-G. Park, "Perovskite solar cells: an emerging photovoltaic technology," *Materials Today*, vol. 18, no. 2, pp. 65–72, Mar. 2015, doi: 10.1016/j.matod.2014.07.007.
- [4] I. Mesquita, L. Andrade, and A. Mendes, "Perovskite solar cells: materials, configurations and stability," *Renewable and Sustainable Energy Reviews*, vol. 82, pp. 2471–2489, Feb. 2018, doi: 10.1016/j.rser.2017.09.011.
- [5] T. Ibn-Mohammed *et al.*, "Perovskite solar cells: An integrated hybrid lifecycle assessment and review in comparison with other photovoltaic technologies," *Renewable and Sustainable Energy Reviews*, vol. 80, pp. 1321–1344, Dec. 2017, doi: 10.1016/j.rser.2017.05.095.
- [6] T.-B. Song *et al.*, "Perovskite solar cells: film formation and properties," *Journal of Materials Chemistry A*, vol. 3, no. 17, pp. 9032–9050, 2015, doi: 10.1039/C4TA05246C.
- [7] J. S. Shaikh *et al.*, "Perovskite solar cells: In pursuit of efficiency and stability," *Materials & Design*, vol. 136, pp. 54–80, Dec. 2017, doi: 10.1016/j.matdes.2017.09.037.
- [8] N. Ahn, D.-Y. Son, I.-H. Jang, S. M. Kang, M. Choi, and N.-G. Park, "Highly reproducible perovskite solar cells with average efficiency of 18.3% and best efficiency of 19.7% fabricated via lewis base adduct of lead(II) Iodide," *Journal of the American Chemical Society*, vol. 137, no. 27, pp. 8696–8699, Jul. 2015, doi: 10.1021/jacs.5b04930.
- [9] J.-H. Im, H.-S. Kim, and N.-G. Park, "Morphology-photovoltaic property correlation in perovskite solar cells: One-step versus two-step deposition of CH<sub>3</sub>NH<sub>3</sub>PbI<sub>3</sub>," *APL MATERIALS*, vol. 2, no. 8, Aug. 2014, doi: 10.1063/1.4891275.
- [10] M. Ozaki *et al.*, "How to make dense and flat perovskite layers for >20% efficient solar cells: Oriented, crystalline perovskite intermediates and their thermal conversion," *Bulletin of the Chemical Society of Japan*, vol. 92, no. 12, pp. 1972–1979, Dec. 2019, doi: 10.1246/bcsj.20190241.
- [11] Peng *et al.*, "High-quality perovskite CH<sub>3</sub>NH<sub>3</sub>PbI<sub>3</sub> thin films for solar cells prepared by single-source thermal evaporation combined with solvent treatment," *Materials*, vol. 12, no. 8, p. 1237, Apr. 2019, doi: 10.3390/ma12081237.
- [12] M. I. Ahmed, Z. Hussain, M. Mujahid, A. N. Khan, S. S. Javaid, and A. Habib, "Low resistivity ZnO-GO electron transport layer based CH<sub>3</sub>NH<sub>3</sub>PbI<sub>3</sub> solar cells," *AIP Advances*, vol. 6, no. 6, Jun. 2016, doi: 10.1063/1.4953397.
- [13] H. J. Snaith *et al.*, "Anomalous hysteresis in perovskite solar cells," *The Journal of Physical Chemistry Letters*, vol. 5, no. 9, pp. 1511–1515, May 2014, doi: 10.1021/jz500113x.
- [14] Q. Chen *et al.*, "Planar heterojunction perovskite solar cells via vapor-assisted solution process," *Journal of the American Chemical Society*, vol. 136, no. 2, pp. 622–625, Jan. 2014, doi: 10.1021/ja411509g.
- [15] F. Hajipour *et al.*, "Developing a fluorescent hybrid nanobiosensor based on quantum dots and azoreductase enzyme formethyl red monitoring," *Iranian Biomedical Journal*, vol. 25, no. 1, pp. 8–20, Jan. 2021, doi: 10.29252/ibj.25.1.8.
- [16] E. A. Al-Oubidy and F. J. Kadhim, "Photocatalytic activity of anatase titanium dioxide nanostructures prepared by reactive magnetron sputtering technique," *Optical and Quantum Electronics*, vol. 51, no. 1, p. 23, Jan. 2019, doi: 10.1007/s11082-018-1738-z.
- [17] B. R. Sankapal, M. C. Lux-Steiner, and A. Ennaoui, "Synthesis and characterization of anatase-TiO<sub>2</sub> thin films," *Applied Surface Science*, vol. 239, no. 2, pp. 165–170, Jan. 2005, doi: 10.1016/j.apsusc.2004.05.142.
- [18] S. El-Sherbiny, F. Morsy, M. Samir, and O. A. Fouad, "Synthesis, characterization and application of TiO<sub>2</sub> nanopowders as special paper coating pigment," *Applied Nanoscience*, vol. 4, no. 3, pp. 305–313, Mar. 2014, doi: 10.1007/s13204-013-0196-y.

- [19] G. Gohari *et al.*, “Titanium dioxide nanoparticles (TiO<sub>2</sub> NPs) promote growth and ameliorate salinity stress effects on essential oil profile and biochemical attributes of *Dracocephalum moldavica*,” *Scientific Reports*, vol. 10, no. 1, p. 912, Jan. 2020, doi: 10.1038/s41598-020-57794-1.
- [20] A. Sharma and N. B. Chaure, “Studies on CH<sub>3</sub>NH<sub>3</sub>PbI<sub>3</sub> prepared by low-cost wet chemical technique,” *Applied Physics A*, vol. 125, no. 11, p. 767, Nov. 2019, doi: 10.1007/s00339-019-3047-1.
- [21] A. Mishra, Z. Ahmad, F. Touati, R. A. Shakoor, and M. K. Nazeeruddin, “One-dimensional facile growth of MAPbI<sub>3</sub> perovskite micro-rods,” *RSC Advances*, vol. 9, no. 20, pp. 11589–11594, 2019, doi: 10.1039/C9RA00200F.
- [22] Y. Bouachiba *et al.*, “TiO<sub>2</sub> thin films studied by FTIR, AFM and spectroscopic ellipsometry,” *International Journal of Nanoparticles*, vol. 6, no. 2/3, p. 169, 2013, doi: 10.1504/IJNP.2013.054992.
- [23] W. Zhang *et al.*, “Solvent-induced textured structure and improved crystallinity for high performance perovskite solar cells,” *Optical Materials Express*, vol. 7, no. 7, p. 2150, Jul. 2017, doi: 10.1364/OME.7.002150.
- [24] Y. Yu *et al.*, “Ultrasoother perovskite film via mixed anti-solvent strategy with improved efficiency,” *ACS Applied Materials & Interfaces*, vol. 9, no. 4, pp. 3667–3676, Feb. 2017, doi: 10.1021/acsami.6b14270.
- [25] S. Wang *et al.*, “Smooth perovskite thin films and efficient perovskite solar cells prepared by the hybrid deposition method,” *Journal of Materials Chemistry A*, vol. 3, no. 28, pp. 14631–14641, 2015, doi: 10.1039/C5TA03593G.
- [26] S. Casaluci *et al.*, “A simple approach for the fabrication of perovskite solar cells in air,” *Journal of Power Sources*, vol. 297, pp. 504–510, Nov. 2015, doi: 10.1016/j.jpowsour.2015.08.010.
- [27] M. Jaysankar *et al.*, “Minimizing voltage loss in wide-bandgap perovskites for tandem solar cells,” *ACS Energy Letters*, vol. 4, no. 1, pp. 259–264, Jan. 2019, doi: 10.1021/acseenergylett.8b02179.

## BIOGRAPHIES OF AUTHORS



**Dwayne Jensen Reddy**     is a Lecturer in the Department of Electrical Power Engineering at the Durban University of Technology in Kwa-Zulu Natal, South Africa where he has been a faculty member since 2010. He joined the South African Technology Network PHD enhancement program in 2020. He completed his Master’s in Engineering and undergraduate studies at the Durban University of Technology. His research interests lie in the area of renewable energy generation, ranging from development of energy generation devices, material fabrication and characterization, PV design and implementation. He is currently a Ph.D. candidate in Engineering at the Durban University of Technology. The provisional title of his research is ‘The effects of Ion doping on the electron transfer layer of Perovskite solar cells’. He can be contacted at email: [dwayner@dut.ac.za](mailto:dwayner@dut.ac.za).



**Prof. Ian Joseph Lazarus**     is an Associate Professor of Physics. He completed his Master’s degree in Nuclear Physics and his doctoral degree focused on linear and nonlinear wave phenomena in electron-positron plasmas. He has a Diploma in Wind Energy Use (Sweden) and has completed courses in advanced renewable energy, advanced energy management, energy optimization and measurement and verification professional. He manages the Energy Technology Station, which focuses on research and innovation in energy and commercialization of energy related products. He also manages a number of community engagement and university projects in the energy field. He conducts research in Renewable Energy and Plasma Physics and supervises masters and doctoral students. His specific field of interest is in solar photovoltaics and solar thin-films, solar thermal, biogas, energy efficiency, figure and building energy. He can be contacted at email: [lazarusi@dut.ac.za](mailto:lazarusi@dut.ac.za).